The Multi-year Predictability of Tropical Pacific Marine Productivity
Supporting Information

Roland Séférian[1,2]*, Laurent Bopp[2], Marion Gehlen[2], Didier Swingedouw[2,3], Juliette Mignot[4,5], Eric Guilyardi[4,6], Jérôme Servonnat[2]

[1] CNRM-GAME/GMGEC - Toulouse, France

[2] IPSL/LSCE - Gif sur Yvette, France

[3] Université de Bordeaux/EPOC – Pessac, France

[4] IPSL/LOCEAN - Paris, France

[5] Climate and Environmental Physics, Physics Institute and Oeschger Centre of Climate Change Research, University of Bern, Switzerland

[6] NCAS Climate, University of Reading – UK

1- Model Description

In this study, we have employed the Earth System Model developed at the Institut Pierre Simon Laplace (IPSL) for the Coupled Model Intercomparison Project phase 5 (CMIP5): IPSL-CM5A-LR (1).

IPSL-CM5A-LR combines the major components of the climate system: the atmosphere and land models are the atmospheric general circulation model LMDZ5A

(2) and the land-surface model ORCHIDEE (3). The atmospheric and land components use the same regular horizontal grid with 96 × 95 points, representing a resolution of 3.75°× 1.87°. The atmosphere has 39 levels on the vertical.

The oceanic component, NEMOv3.2 (2, 4), offers a horizontal resolution of 2° refined to 0.5° in the tropics and 31 vertical levels. NEMOv3.2 is coupled to the sea ice model LIM2 (5) and the marine biogeochemistry model PISCES (6).

PISCES simulates the biogeochemical cycles of carbon, oxygen and nutrients using 24 state variables. Macronutrients (nitrate and ammonium, phosphate, and silicate) and the micronutrient iron limit phytoplankton growth and thus improve the representation of their dynamics (6, 7). Inorganic carbon pools are dissolved inorganic carbon, alkalinity and calcite. Total alkalinity includes contributions from carbonate, bicarbonate, borate, hydrogen, and hydroxide ions (practical alkalinity). For dissolved CO2 and O2, air-sea exchange follows the quadratic wind-speed formulation (8)

PISCES distinguishes two classes for phytoplankton (nanophytoplankton and diatoms), for which growth is parametrized using the (9) formulation but limited by external availability of nutrients. Diatoms differ from nanophytoplankton because they need silicon and more iron (10) and because they have higher half-saturation constants due to their larger mean size. In PISCES, zooplankton is described by two size classes: microzooplankton and mesozooplankton. The ratios between carbon, nitrate, and phosphate are considered constant and held to the values proposed by (11) for all plankton classes. However, internal concentrations of iron are simulated prognostically in both phytoplankton classes, as is silica in diatoms. Phytoplankton growth depends on external concentrations of nutrients and light availability, while chlorophyll concentration is simulated prognostically following (12).

2- Data

2-1 Sea Surface temperature

In this study, we used two observed datasets for sea surface temperature (SST) in order to account for observational uncertainties in our skill-score estimates. The two datasets we considered are those described in (13) and (14).

2-2 10 meters winds

Zonal winds at 10 meter were used in the study in order to assess benefits of

initialization. For this purpose, we employed product provided by the NCEP reanalyses described in (15).

2-3 Net Primary Productivity

Similarly to SST, we used several estimates of NPP that were derived from satellite measurements of SeaWiFS (1997-2008) and MODIS (2002-2012) and the VGPM (16) and Eppley-VGPM algorithms (17). These products are developed at the Oregon State University: http://www.science.oregonstate.edu/ocean.productivity/index.php.

2-4 Skipjack Tuna Catch Biomass

Data were collected from purse seine for Skipjack Tuna from 1991 to 2012 over the Tropical Pacific (30°S-30°N). These data were provided by the IATTC and the WCPFC for respectively the Eastern part and the Western part of the Pacific Ocean. Catch per units were combined into a 1°x1° grid on the basis of the following criteria:

- monthly data
- no domestic fisheries is not included
- cell grid representing less than three vessels are excluded (the umber of vessels taken into account in a 1°x1° grid roughly reduces by half compared to those considered for a 2°x2° grid)

The two datasets are then

- combined in a 1°x1° regular Mercator grid

Considering that the last criterion has large consequences on the biomass catch estimates, we have conducted a basic assessment of the resolution of the two datasets. Correlation between estimated oscillations for catch biomass estimated from the 1°x1° gridded dataset and those estimated from the 2°x2° gridded dataset reaches up to 0.8 which shows the rather good agreement of the two gridded datasets.

3- Experimental Design

3-1- Spin-up

As explained in (1) and (18), IPSL-CM5A-LR has been spun-up for several century in order to produce initial state for both dynamical and biogeochemical components of

the Earth System Model.

Spin-up strategy follows the sequential steps:

(1) After initialisation with modern climatologies, a first online spin-up is performed with the dynamical components (atmosphere, oceans, sea-ice, land surface) only for 600 years with fixed preindustrial condition (19).

(2) Once the climate of the model is steady, a climatology of the last 50 years is computed in order to forced the biogeochemical components of the land and the oceans offline. After initialisation with observed climatologies of nutrients, carbon-related fields and oxygen, PISCES is spun-up offline for 3000 years for marine biogeochemistry.

(3) The initial conditions for marine and land biogeochemical reservoirs performed in step (2) are used to initialised the marine and land components of IPSL-CM5A-LR. Once, all the components are initialised, IPSL-CM5A-LR is run for an other 330 years for online adjustment.

3-2- The non-initialized simulation

In this study, the non-initialized simulation corresponds to one member of the historical simulations ensemble performed with IPSL-CM5A-LR for CMIP5 (19). This means that IPSL-CM5A-LR is forced by observed changes in the atmospheric chemical composition (natural and anthropogenic green house gases and aerosols), solar constant and land use between 1850 and 2005. Initial conditions come from the sequential spin-up explained above.

From 2005 to 2011, IPSL-CM5A-LR is forced by changes in atmospheric chemical composition following the Representative Concentration Pathway 4.5 (RCP45) according to CMIP5 decadal framework except for the volcanoes background that has been removed here.

3-3- The initialized simulation

As explained, although Earth system models are able to capture the relationship between NPP and climate-state, the phasing and the amplitude of these variations are poorly reproduced in non-initialized simulations. To partly overcome this difficulty, we took advantage of the initialization strategy used at the IPSL and apply for the first

time to an Earth System Model: IPSL-CM5A-LR. This simple initialization scheme, developed for seasonal forecast, consists of relaxing SST anomalies of the IPSL-CM5A-LR to observations. The nudged simulation has thus been performed by relaxing SST anomalies of the IPSL-CM5A-LR to (13) reconstruction between 1949 to 2011 with a restoring coefficient of 40 $W/m^2/K$

This methodology was employed at IPSL for CMIP5 decadal framework to smoothly phase IPSL-CM5A-LR variability with the observed one. With IPSL-CM5A-LR, (20) demonstrated that this initialization strategy gives encouraging results for the prediction of the Atlantic meridional overturning circulation in the CMIP5 decadal framework (accounting for volcanoes background).

3-3- The hindcasts

The initialized simulation provides initial or starting conditions for a set of ten-year-long, three-member ensemble hindcasts that are performed every years from 1987 to 2001 to cover the 1997-2011 period (Figure S1 for NPP and S2 for SST). There is no SST restoring during the ten years of simulations for the hindcasts (meaning that the model is not guided anymore by observed SST anomalies in these simulations).

As in (20), the hindcasts ensemble is created by applying a white noise perturbation on SST from the nudged simulation with an anomaly that has been chosen randomly for each grid points in the interval ±0.05°C. Grid points under sea-ice cover are not perturbed. Note that this hindcast ensemble follows the same set up as the hindcasts published for the short-term CMIP5 experiment except that the background volcanic aerosols imposed from 2006 onward in the scenario RCP45 is not imposed here.

3-4- Sensitivity experiments in a perfect model framwork

The experimental set-up of these sensitivity experiments relies on several ensemble model simulations. The reference simulation consists in a 1000-year-long preindustrial simulation of IPSL-CM5A-LR (1800-2799 in model years). Ten 20-years-long ensembles simulations were performed for five starting dates: 1901, 2056, 2066, 2071 and 2171. Ensemble simulations were generated by applying a random noise in a range of [-0.05—0.05] °C uniformly on the oceanic sea surface temperature. This experimental set-up has been widely used and is detailed in (21).

4- Statistical Methods

4-1- Post-treatments

Each simulations used in this study has been regridded on a regular Mercator (or regular) grid of 1°x1° of resolution. Annual anomalies are computed after removing a linear drift for all lead times of the hindcasts. Monthly anomalies are computed after removing mean seasonal cycle computed over the whole period (1991-2012).

4-2- Skill-score

Two skill-scores are used in this study: the anomaly correlation skill-score and the root-mean-square skill-score. They are both widely employed in seasonal and decadal forecast to assess model predictions against observations.

Skill-score computation are performed by comparing observed time series against a "reconstituted" time series, which is composed by the years of the hindcasts pending on the lead time as presented in the Figure S3. This methodology has been introduced by (22) for assessing benefits of initialization on North Atlantic surface temperature. Further explanations on this method, which is widely used to assess decadal predictions, are available in (23, 24). Here, hindcasts are performed in order to conserve the length of the observed time series. That is, hindcasts are conducted retrospectively as presented on the Figure S3.

Following this methodology, the anomaly correlation skill-score between model prediction (p) and observations (o) over N years is computed as follows:

$$AC-SS=\frac{1}{N}\frac{\sum(p-\overline{p})(o-\overline{o})}{\sum(p-\overline{p})^2\sum(o-\overline{o})^2}$$

Where the bar indicates the temporal averaging operator.

The significance of the AC-SS is tested against a two-tailed t-test with N-2-1 degree of freedom (that is also estimated with Bretherthon's formulae (25)).

The root-mean-square error skill-score is given by:

$$RMSE-SS=\frac{1}{N}\sum\left[(p-\overline{p})-(o-\overline{o})\right]^2$$

The RMSE-SS is tested against the standard deviation of the observations. This means that the ensemble is spread is assessed against the observed variations of a given variable.

5- Mechanisms of initialization

In this section, we briefly describe how marine productivity has been initialized trough SST nudging.

Figure S4 shows correlations of monthly deseasonalized for SST, surface zonal winds and NPP of the observation-derived datasets with the initialized simulation on the one hand, and with the non-initialized simulation on the other hand. This allows to assess the benefits of the initialization scheme for SST, surface zonal winds and marine productivity. On Figure S4, it appears clearly that SST nudging improves phasing and amplitude of simulated surface zonal winds and NPP in the Tropical Pacific (30°S-30°N), where correlations are significantly different from zero at 95% confidence level. Similar patterns are not apparent on the non-initialized simulation. Surface zonal winds are thus initialized through SST restoring within the Tropical Pacific. This is explained by the fact that SST nudging improves the representation of the meridional gradient of SST and consequently sea-level pressure though air-sea exchanges inducing a correction of the surface zonal winds thanks to the thermal winds imbalance.

A simplified scheme is proposed in Figure S5 to explain mechanisms we suggest to be responsible of NPP initialization. On this scheme, we suggest that NPP variability has been substantially improved in term of variability in response to two pathways: one related to ocean dynamics and the other to biogeochemical dynamics.

First, the dynamical pathway represents the dynamical adjustment of the winds to the more realistic meridional SST gradients (and its temporal variability). This dynamical adjustment leads to a better representation of zonal winds over a large fraction of the Tropical Pacific (26). Since variations of surface zonal winds are initialized through SST nudging, the variations of the upwelling of the Eastern Equatorial Pacific is better represented in the initialized simulation compared to that of the non-initialized one. The upwelling replenishes surface nutrients during the La Niña events, which stimulates growth of phytoplankton, and hence leads to a better representation of the

spatiotemporal variability of the NPP.

Second, the biogeochemical pathway concerns the fact that the marine biology is also directly affected by SST and therefore SST nudging. This latter modifies the growth rate of phytoplankton and the grazing rate of zooplankton, both related to environmental temperature. This response occurs also at short time scale and represents the quickest adjustment of marine biogeochemistry to SST nudging. Compared to the dynamical pathway, the biogeochemical response is of a lesser importance. Nevertheless, the biogeochemical pathway still contributes to the phasing of NPP variations to those of SST in response to the various ENSO events.

Figure S6 illustrates impacts of SST restoring on the mixed-layer depth (as proxy of the Equatorial upwelling) and the surface nutrients (dissolved iron and nitrate). On this Figure, variations of surface nutrients, mixed layer depth and SST averaged over the tropical Pacific are stronger in the nudged simulations than in the free run; their timing are also consistent with the various ENSO events represented by the Nino3.4 index (Figure S6d).

In this work, we hypothesize that initialization of surface zonal winds ensure a better representation of the upwelling Eastern Equatorial Pacific. To investigate the validity of this hypothesis, we computed monthly cross-correlations between variations of the mixed layer depth averaged over the Tropical Pacific and SST, nutrients and NPP respectively averaged and integrated over the Tropical Pacific (considered here as co-variables). Figure S7 shows the results of these computations. On this Figure, strong positive (negative) correlations at negative time lags indicate that the mixed layer fluctuations leads positive (negative) anomalies of the given co-variables. On the contrary, positive time lags indicate that anomalies of the given co-variables take the lead of the mixed layer fluctuations.
Figure S7 shows that variations of the mixed layer depth drives changes in SST and surface nitrate concentration within a month, while it influences NPP and dissolved iron at seasonal timescale (6-8 months). This confirms that variations of the upwelling tend to control subsequent variations of SST and biological elements.

Finally, the repartition of nutrient supply due to vertical mixing in response to the

variations of the upwelling and due to the regenerated loop of nutrients (through the remineralization of the organic matter) of nutrients ensures a good representation of the magnitude and the phasing of the Tropical Pacific NPP during the various ENSO events (Figure S8). For this analysis, we have recomputed offline the regenerated and preformed nitrate from apparent oxygen utilization (AOU). We have employed this proxy since in our model, PISCES (6) remineralization of dissolved organic matter can occur within both oxic and anoxic waters. The splitting between the two types of organic matter degradation depends on the local oxygen concentration with a threshold fixed in time to 6 micromoles per liter. This formulation assumes implicitly that the degradation rates for oxic respiration and denitrification are identical.

On this Figure, we show the variance of regenerated nitrate and preformed nitrate integrated between the surface and 100 m. From this Figure, we demonstrate that the spatiotemporal distribution of preformed nitrate differs from that of regenerated nitrate. Such repartition results from the fact that lateral advection of preformed nitrate is more pronounced than that of regenerated nitrate (Figure S8ab). However, regions away from the influence of the Equatorial upwelling (20°S-20°N) exhibit a stronger sensitivity to the recycling processes than the vertical supply of preformed nutrients, especially in the Northern part of the Tropical Pacific. Such a repartition is consistent with previous studies performed with regional model forced by atmospheric observations (27). In term of phasing, anomalies of regenerated and preformed nitrate are generally out of phase, but seem to be both driven by the various El Niño/La Niña events.

Of this Figure, we can conclude that the nitrate variability within the Tropical Pacific is prominently governed by an upwelling-driven nutrients supply. Nonetheless,

recyclcing processes seem to play a substantial role for a fraction of Tropical Pacific area away from the Equatorial tongue. Such mechanisms potentially play a role in the persistence of nutrients and NPP anomalies as well as in the predictability of NPP.

6- Persistence: property responsive of differences in predictive skill

As pointed out in the main text, mechanisms explaining the largest predictability for NPP rely on the fact that the biogeochemical system exhibits a longer memory than the SSTs.

To evaluate these differences, we computed normalized spectral density for NPP, SST and surface chlorophyll (Chl) from the 1000 years of the spin-up simulation of IPSL-CM5A-LR. This simulation provides a sufficient number of decades to accurately determine low-frequency modes of variability (28). It does not include the influence of external forcings (like anthropogenic climate change), which could favor the emergence of low frequency modes of variability for SST (due to global warming) compared to NPP. Figure S9 presents the normalized wavelet power spectrum for yearly time series of NPP, Chl and SST averaged over the Tropical Pacific. It proves the existence of low frequency variations for Chl and NPP, which share common features in terms of variations and amplitude between the 30-year and 130-year periods (multi-decadal time scales). SST variations in the Tropical Pacific are confined to time scales smaller than 30 years, and hence reveal the prominent influence of ENSO events at the interannual time scale.

We estimated how the existence of long-term memory properties could affect predictability by computing persistence (auto-correlation function). The computation of persistence relies on the simplest statistical model mimicking memory in a dynamical system (29). It is called a first order auto-regressive model (AR1) and can be written as follows:

$\frac{dX(t)}{dt} = \alpha X(t) + \varepsilon(t)$ where $X(t)$ is a time evolving variable, $\varepsilon(t)$ is a Gaussian white noise and $1/\alpha$ is analogous to time.

Computation of the persistence allows estimating α, which is the auto-correlation

coefficient. When α is significantly equal to zero, the memory of the system is considered loss.

Figure 3 in the main text compares the persistence of yearly anomalies of SST, surface concentrations of nitrate and dissolved iron and NPP. This Figure shows that the NPP, nitrate and dissolved iron anomalies exhibit a larger persistence than the SSTs. This result supports the hypothesis of a longer memory of the biogeochemical system compared to SST in the Tropical Pacific. It suggests consequently that benefits of initialization are kept over several years for NPP and surface nutrients, not for SST. The persistence is a useful baseline to evaluate whether the model can produce a better prediction than the climatology elsewhere (20, 22, 30). In our case, we have shown that biogeochemical system (nutrients and NPP) exhibits a longer memory than SST independently from the use of a simple statistical model (AR1) or with a complex Earth System Model. This demonstrates that our model does a better job in predicting natural variations of NPP than an AR1 process based on the NPP climatology.

Differences in terms of predictability between the AR1 and the complex Earth System model are partly attributable to oceanic transport. Figure 4 illustrates how anomalies of NPP induced by variations of the Equatorial upwelling are propagated poleward in course of time. Same lagged correlations are found for surface nitrate and dissolved iron (Figure 3).

7- Evaluating robustness of NPP predictability horizon

We applied two different approaches in order to assess the robustness of our estimation of the predictability horizon for NPP:
First and in order to evaluate its robustness with the respect to the satellite-derived NPP product, we performed the same analysis for the NPP estimated from the MODIS measurements over the 2002-2012 period. Results are summarized on Figure S10. This figure presents the same skill-score diagram as on Figure 2c but for the NPP derived from MODIS. AC-SS and RMSE-SS found over this period are slightly lower than those corresponding to the SeaWiFS period. However, the estimate of the

effective predictability horizon of ~3 years is robust.

The second approach follows a method widely employed in the community and called "the perfect model framework" in order to conduct an in-depth evaluation of the net primary productivity potential predictability skill-scores. The philosophy of this approach relies on the sensitivity of the model to perturbations in initial conditions. The initial perturbation is supposed to represent atmospheric chaotic noise or uncertainty in the estimation of the climate state (31, 32) This approach represents an estimate of the upper limit of predictability based on having a perfect model and near perfect knowledge of the current state of the climate system (principally the state of the ocean). Although this situation is never likely to be achieved in practice, this approach is useful in identifying explicitly the climate predictability over a specific climate trajectory. In addition, this framework enables a complete description and sampling of the climate system.

In this framework, model predictive skill is assessed with the metrics described in (33). This metrics is analogous to a root-mean-squared error. The RMSE, (Equation 1) used by Msadek et al. (2010) considers the ensemble mean as baseline. Considering X_i as the ith member of the M members of the ensemble (M=10) and $\overline{X}$ as the ensemble mean, we express RMSE as follows:

$$RMSE = \sqrt{\frac{1}{M}\sum_{i=1}^{M}(X_i(t) - \overline{X}(t))^2} \sim \mathrm{N}(0, \sigma^2) \qquad (1)$$

Based on the perfect model framework analysis (Figure S11), we find that the predictability horizon for NPP varies in function of the starting dates. As such, this result demonstrates the sensitivity of the predictive skill to initial climate state (ENSO events). Nonetheless, this sensitivity is weak in average considering that only one of the five initial conditions has substantially altered the predictability of NPP. In average, the latter is estimated to 5.6 years across the five starting dates.

This analysis shows that the 8-year-long predictability horizon is clearly the upper limit of predictability that can be expected from our model. The lower limit of the NPP predictability horizon is slightly higher than that found for SST (1 year). The lower limit is also comparable to result obtained for the NPP over the MODIS period

(Figure S10), which shows 3 years of potential predictability.

The fact that our effective predictability horizon estimated from satellite-derived observations falls within the distribution of potential predictability horizon diagnosed from a more exhaustive experimental setup (10 members for each starting date) demonstrates its robustness.

References:

1. Dufresne J-L et al. (2013) Climate change projections using the IPSL-CM5 Earth System Model: from CMIP3 to CMIP5. *Clim Dyn* 40:2123–2165.

2. Hourdin F et al. (2013) Impact of the LMDZ atmospheric grid configuration on the climate and sensitivity of the IPSL-CM5A coupled model. *Climate Dynamics* 40:2167–2192.

3. Krinner G et al. (2005) A dynamic global vegetation model for studies of the coupled atmosphere-biosphere system. *Global Biogeochem Cycles* 19:1–33.

4. Madec G (2008) *NEMO ocean engine* (Institut Pierre-Simon Laplace (IPSL))Institut Pierre-Simon Laplace (IPSL), France. Available at: http://www.nemo-ocean.eu/About-NEMO/Reference-manuals.

5. Fichefet T, Maqueda MAM (1997) Sensitivity of a global sea ice model to the treatment of ice thermodynamics and dynamics. *J Geophys Res* 102:12609–12646.

6. Aumont O, Bopp L (2006) Globalizing results from ocean in situ iron fertilization studies. *Global Biogeochem Cycles* 20:GB2017.

7. Aumont O, Maier-Reimer E, Blain S, Monfray P (2003) An ecosystem model of the global ocean including Fe, Si, P colimitations. *Global Biogeochem Cycles* 17:1060.

8. Wanninkhof R, McGillis WR (1999) A cubic relationship between air-sea CO_2 exchange and wind speed. *Geophysical Research Let* 26:1889–1892.

9. Eppley RW, Rogers JN, McCarthy JJ (1969) Half-Saturation Constants for Uptake of Nitrate and Ammonium by Marine Phytoplankton. 14:912–920.

10. Sunda W, Huntsman S (1997) Interrelated influence of iron, light and cell size on marine phytoplankton growth. *Nature* 390:389–392.

11. Takahashi T, Broecker W, Langer S (1985) Redfield Ratio Based on Chemical-Data From Isopycnal Surfaces. *Journal of Geophysical Research-Oceans* 90:6907–6924.

12. Geider R, MacIntyre H, Kana T (1998) A dynamic regulatory model of phytoplanktonic acclimation to light, nutrients, and temperature. *Limnology and Oceanography* 43:679–694.

13. Reynolds RW, Rayner NA, Smith TM, Stokes DC, Wang W (2002) An Improved In Situ and Satellite SST Analysis for Climate. *J Climate* 15:1609–1625.

14. Rayner NA et al. (2003) Global analyses of sea surface temperature, sea ice, and night marine air temperature since the late nineteenth century. *J Geophys Res* 108:4407.

15. Kistler R, Kalnay E, Collins W, Saha S (2001) The NCEP-NCAR 50-year reanalysis: Monthly means CD-ROM and documentation. *Bulletin-American* ….

16. Behrenfeld MJ, Falkowski PG (1997) Photosynthetic rates derived from satellite-based chlorophyll concentration. *Limnology and Oceanography* 42:1–20.

17. Behrenfeld MJ (2005) Carbon-based ocean productivity and phytoplankton physiology from space. *Global Biogeochem Cycles* 19.

18. Séférian R et al. (2013) Skill assessment of three earth system models with common marine biogeochemistry. *Climate Dynamics* 40:2549–2573.

19. Taylor KE, Stouffer RJ, Meehl GA (2009) *A Summary of the CMIP5 Experiment Design* (International CLIVAR Project Office). 2009 Ed.

20. Swingedouw D, Mignot J, Labetoulle S, Guilyardi E, Madec G (2013) Initialisation and predictability of the AMOC over the last 50 years in a climate model. *Clim Dyn* 40:2381–2399.

21. Persechino A, Mignot J, Swingedouw D, Labetoulle S, Guilyardi E (2013) Decadal predictability of the Atlantic meridional overturning circulation and climate in the IPSL-CM5A-LR model. *Clim Dyn* 40:2359–2380–2165.

22. Keenlyside NS, Latif M, Jungclaus J, Kornblueh L, Roeckner E (2008) Advancing decadal-scale climate prediction in the North Atlantic sector. *Nature* 453:84–88.

23. Meehl GA et al. (2009) Decadal Prediction. *Bull Amer Meteor Soc* 90:1467–1485.

24. Meehl GA et al. (2013) Decadal Climate Prediction: An Update from the Trenches. *Bull Amer Meteor Soc*.

25. Bretherton CS, Widmann M, Dymnikov VP, Wallace JM, Bladé I (1999) The

Effective Number of Spatial Degrees of Freedom of a Time-Varying Field. *J Climate* 12:1990–2009.

26. Servonnat J et al. (2014) Reconstructing the subsurface ocean decadal variability using surface nudging in a perfect model framework. *Clim Dyn*:1–24–24.

27. Wang XJ, Murtugudde R, Le Borgne R (2009) Nitrogen uptake and regeneration pathways in the equatorial Pacific: a basin scale modeling study. *Biogeosciences* 6:2647–2660.

28. Séférian R, Bopp L, Swingedouw D, Servonnat J (2013) Dynamical and biogeochemical control on the decadal variability of ocean carbon fluxes. *Earth Syst Dynam* 4:109–127.

29. Frankignoul C (1985) Sea surface temperature anomalies, planetary waves, and air-sea feedback in the middle latitudes. *Rev Geophys* 23:357–390.

30. Matei D et al. (2012) Multiyear Prediction of Monthly Mean Atlantic Meridional Overturning Circulation at 26.5 N. *Science* 335:76–79.

31. Collins M, Sinha B (2003) Predictability of decadal variations in the thermohaline circulation and climate. *Geophys Res Lett* 30:1306.

32. Msadek R, Dixon KW, Delworth TL, Hurlin W (2010) Correction to "Assessing the predictability of the Atlantic meridional overturning circulation and associated fingerprints." *Geophys Res Lett* 37.

33. Msadek R, Dixon KW, Delworth TL, Hurlin W (2010) Assessing the predictability of the Atlantic meridional overturning circulation and associated fingerprints. *Geophys Res Lett* 37.

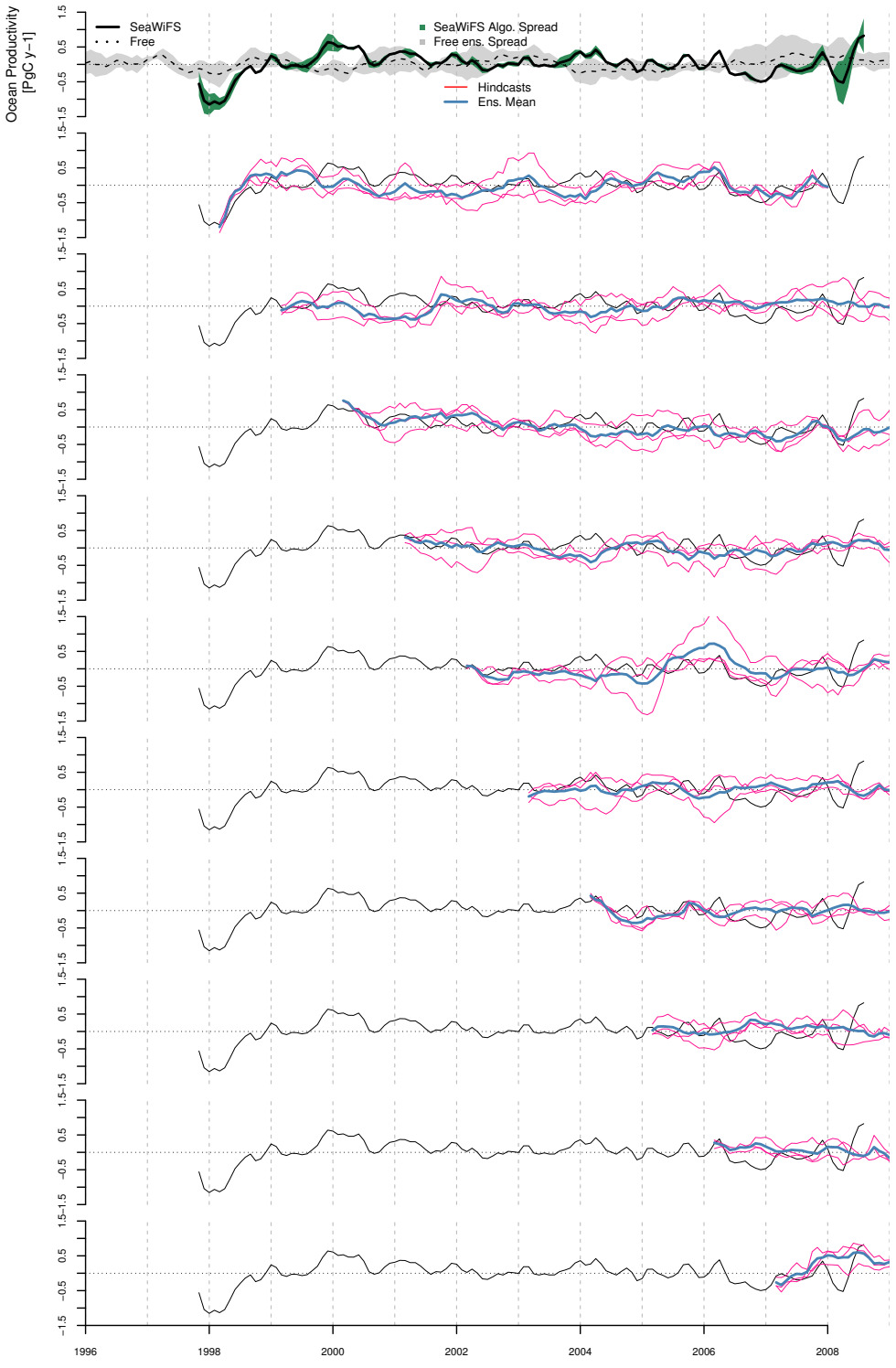

FIGURE 1 – Multiyear anomalies of marine productivity hindcasts compared with satellite-derived observations and free climate model simulations over the SeaWiFS (1997-2008) and MODIS (2003-2011) periods within the low-latitude Pacific oceans (30°S-30°N). Estimates spread from VGPM and Epply-PM algorithms are given in green and the algorithm mean is shown in black ; the individual hindcasts and their ensemble mean are shown in blue and red, respectively. Anomalies of marine productivity from the free climate simulations is shown in the upper plots in dashed black lines for individual experiments and with grey shading for the CMIP5 5 members ensemble mean.

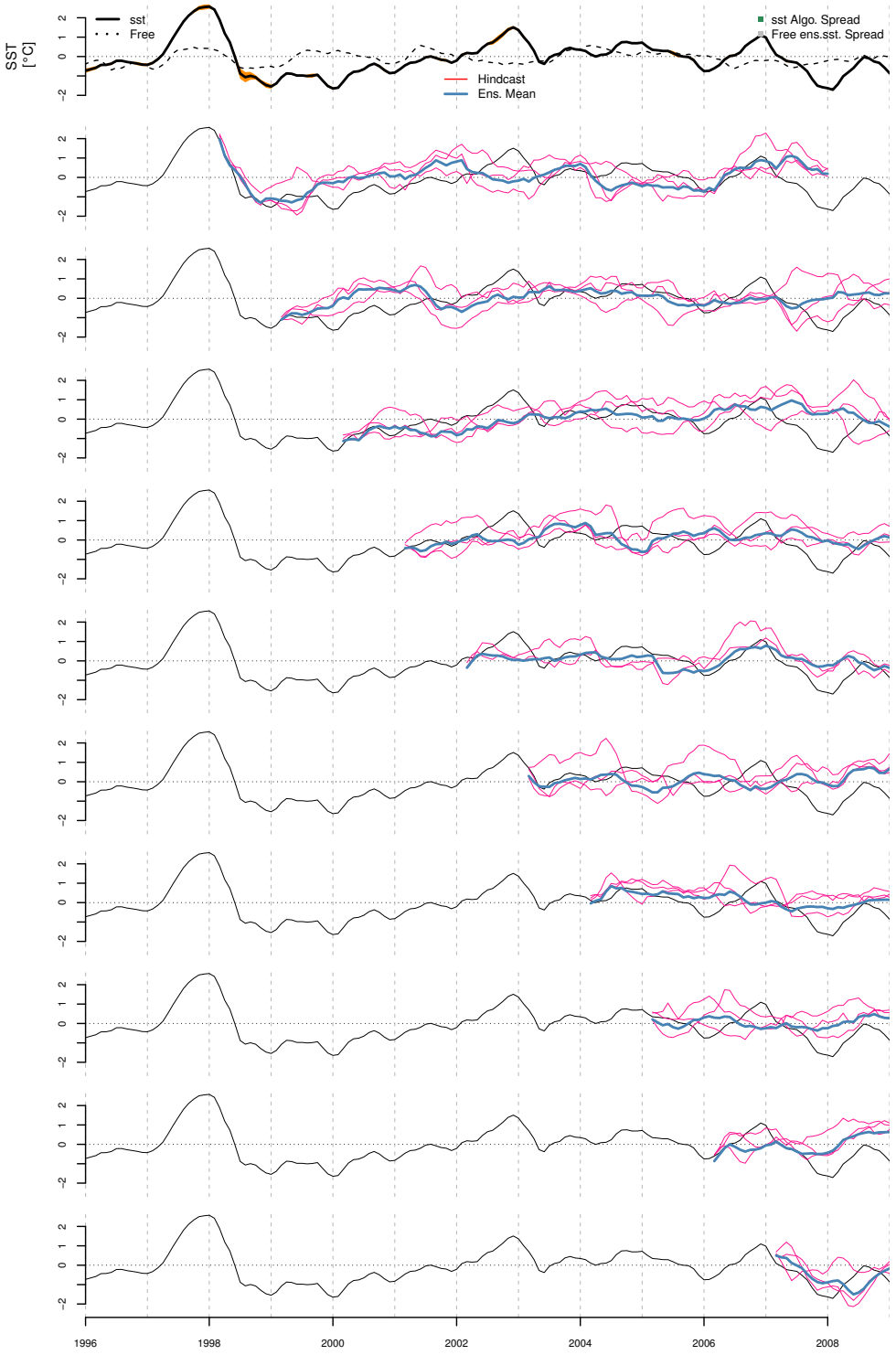

FIGURE 2 – As Figure 1, but for SST over the whole 1997-2011 period.

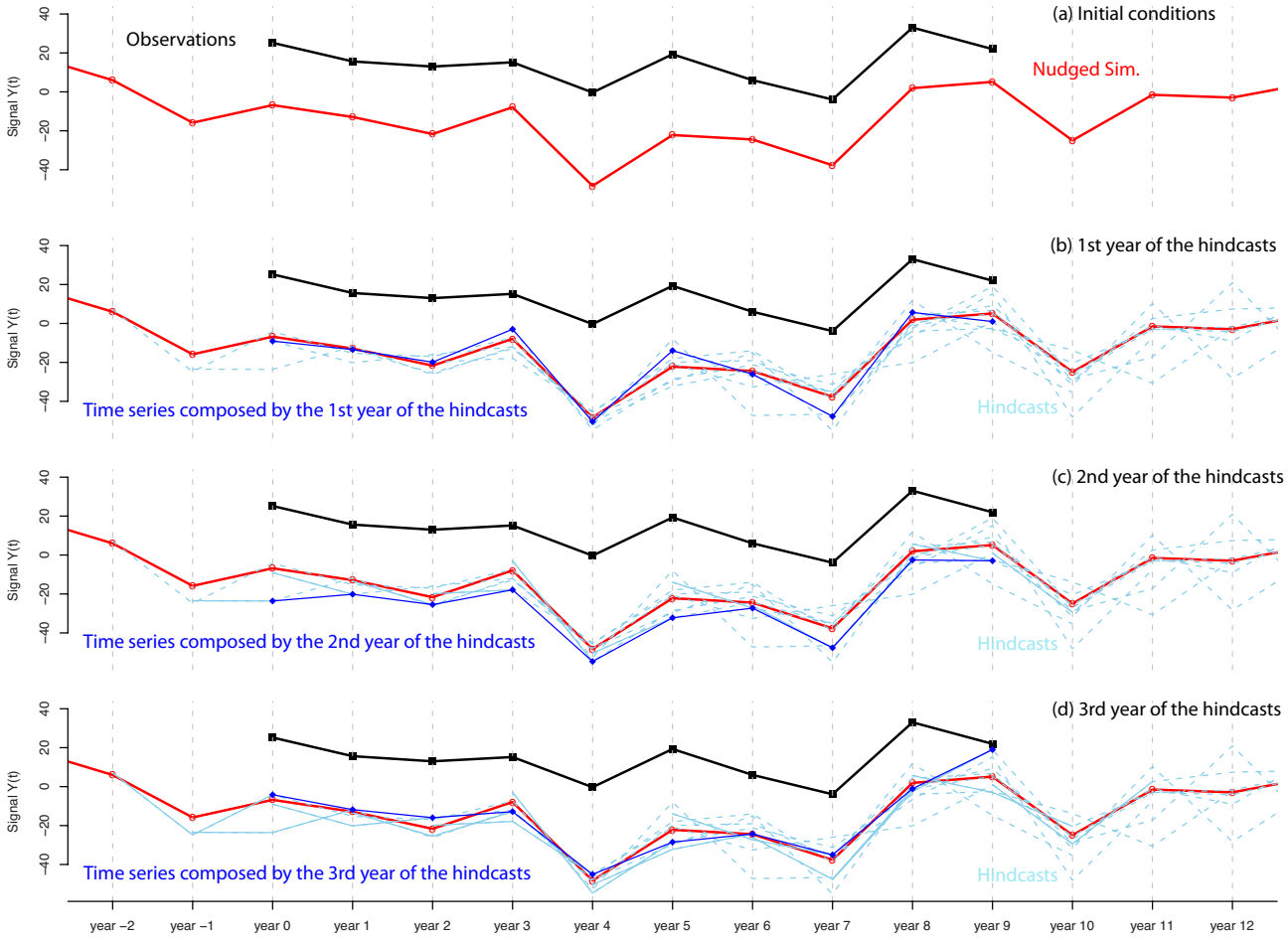

FIGURE 3 – Simplified schema describing how benefits of initialization has been estimated. The observations (in solide black line) are only available over ten years. Nudged simulation (in solid red line) is directly comparable to the observations time series. This simulation provides initial/starting condition for the hindcasts (here, the dashed lines in skyblue). Initial/starting conditions are indicated by small red circles. Benefits of the initialization is estimated by combining the n year of the hindcasts ($n = 1, 2...10$) into a reconstituted time serie (in solid blue line). Here, the scheme illustrated reconstituted time serie for the first year, the second year and the third year of the hindcasts, namely lead time 1, 2 and 3 (with the abreviations LT1, LT2 and LT3). Anomaly Correlation Skill Score (AC-SS) and Root Mean Square Error Skill Score (RMSE-SS) are computed by using observations/Nudged simulations and the reconstituted time serie at the different lead time.

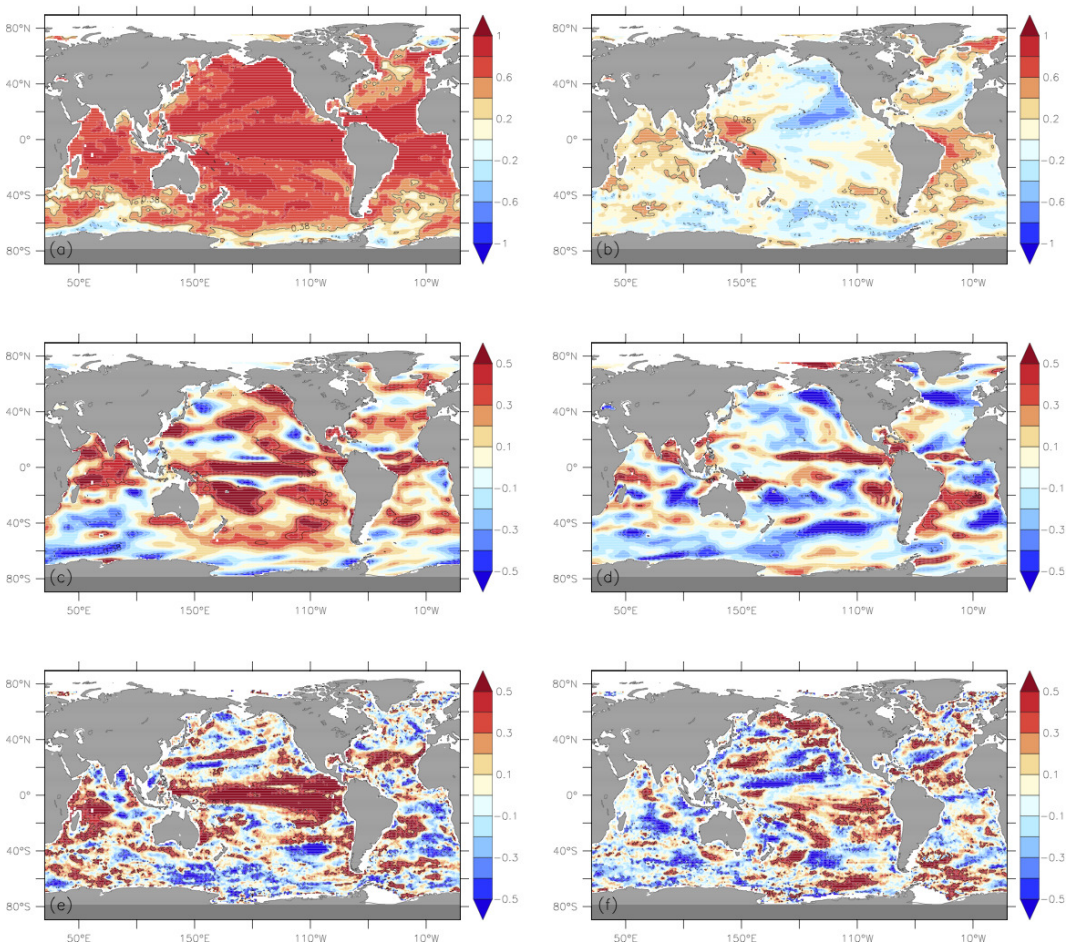

FIGURE 4 – Assessement of benefits from initialization : Comparison of monthly anomalies correlations between the observed dataset and the nudged simulation against the free simulation for (a)-(b) SST, (c)-(d) zonal 10 meters winds abd (e)-(f) NPP. Correlations that passes a two-tailed t-test at 95% significance level are countoured. Observed datasets are Reynolds et al., (2002) for the SST, VGPM algorithm on the basis of SeaWiFS measurements for the NPP and Kistler et al., (2001) for the NCEP2 zonal 10 meters winds.

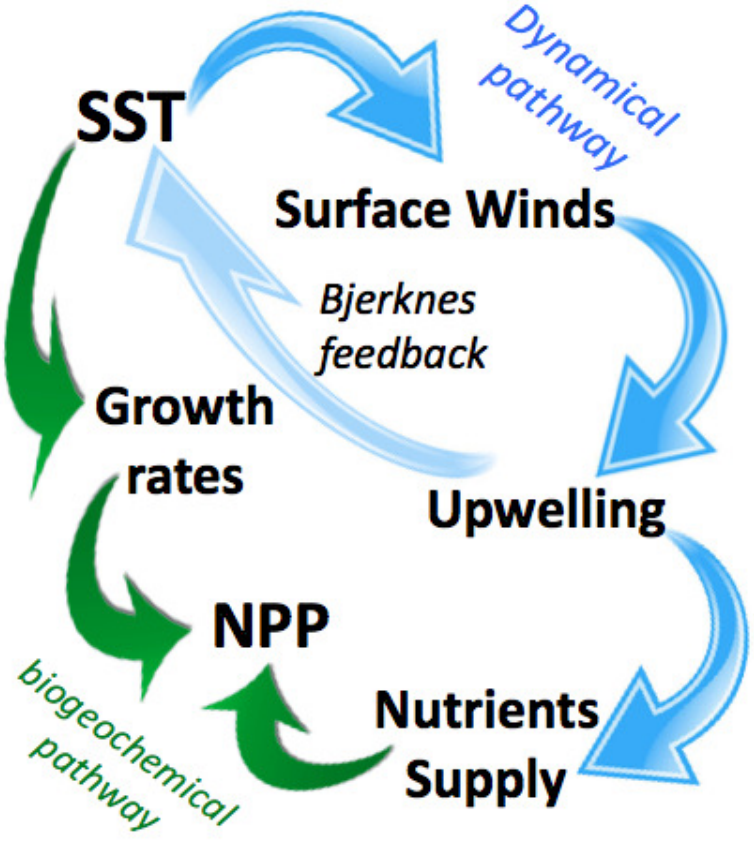

FIGURE 5 – Simplified scheme of NPP initialization through SST restoring. Response of ocean physics and biogeochemistry in the Tropical Pacific (30°S-30°N) to SST nudging is given in blue and green respectively.

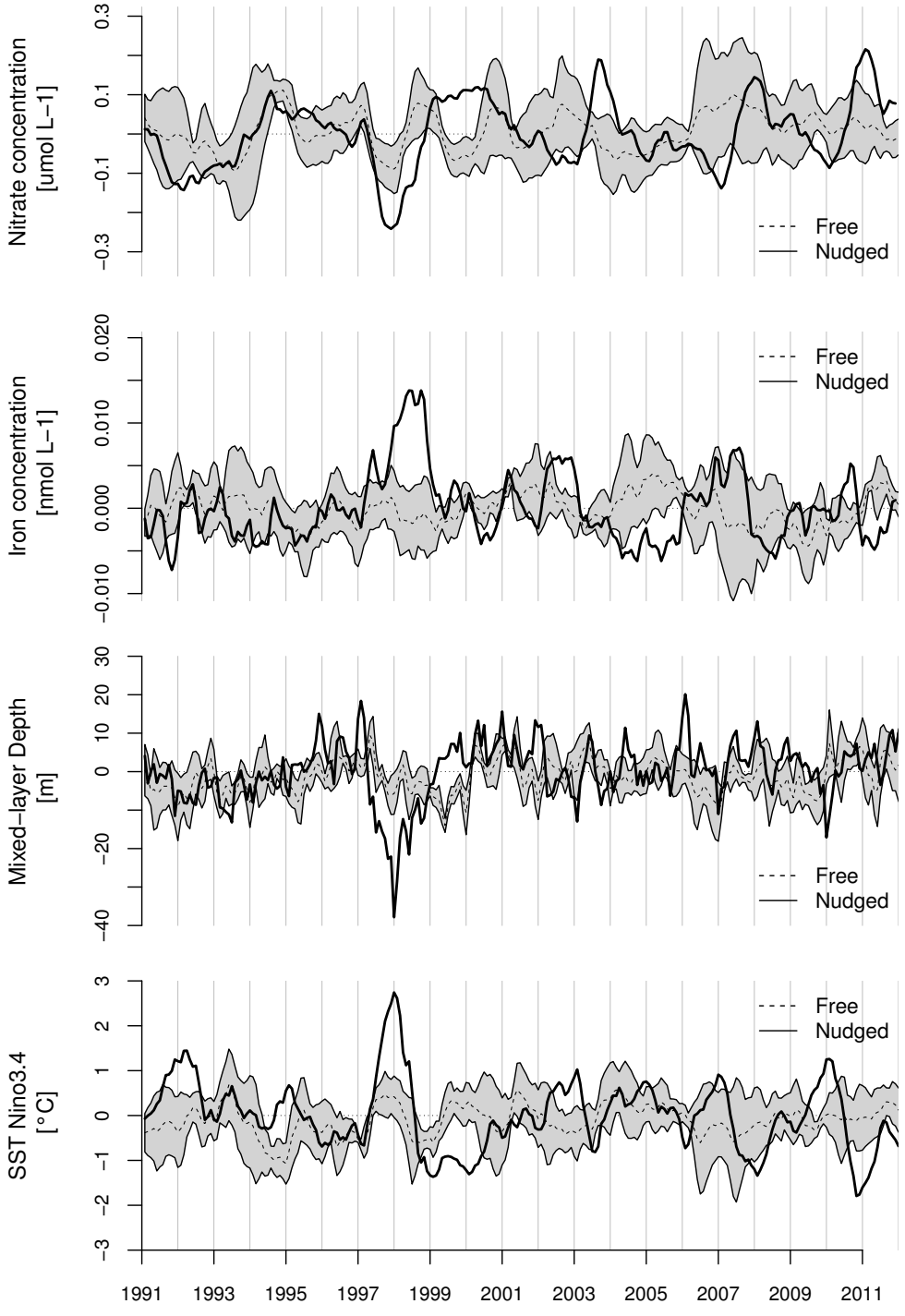

FIGURE 6 – Monthly anomalies of surface concentrations of (a) nitrate and (b) iron, (c) mixed-layer depth and (d) Nino3.4 SST index averaged over the 30°S-30°N Pacific ocean. Grey shading represents the free CMIP5 5 members spread for iron, nitrate, mixed-layer depth and Nino3.4 SST index. Dashed and bold lines indicate free CMIP5 5 members ensemble mean and nudged simulation, respectively.

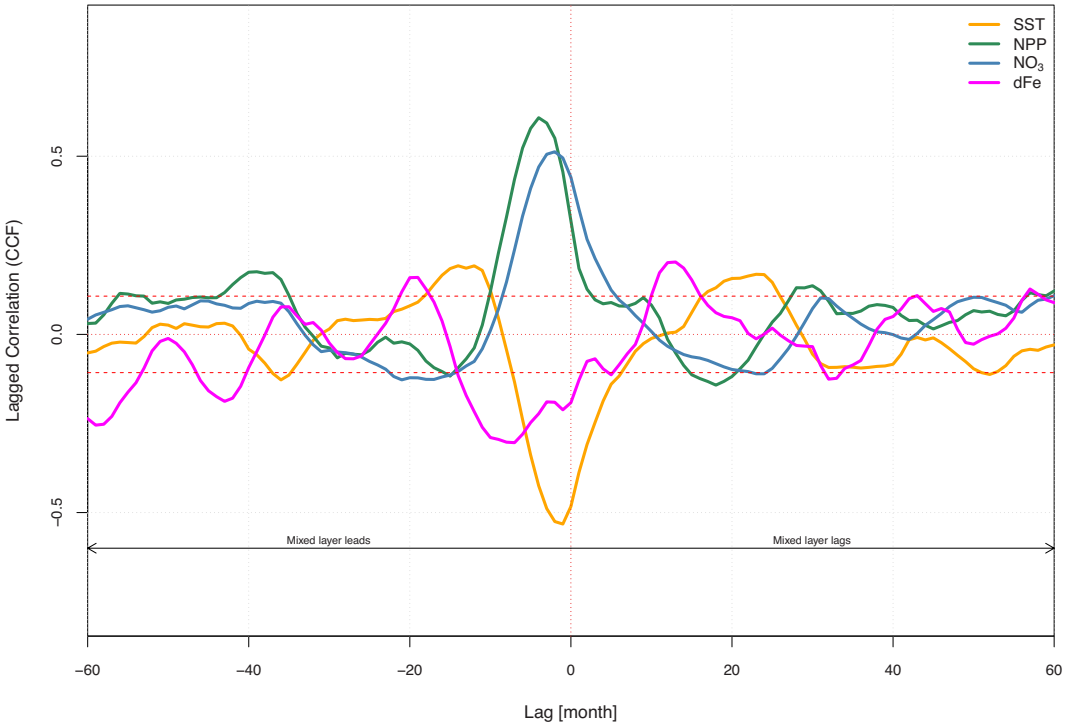

FIGURE 7 – Temporal cross correlations over the 1991-2011 period between variations of mixed-layer and sea surface temperature (SST), net primary productivity (NPP) and surface concentrations of nutrients (NO_3 and dFe) within 30°S–30°N Pacific. The null hypothesis of a zero correlation is tested against a t-test at 95% significance level and is indicated with red dashed lines.

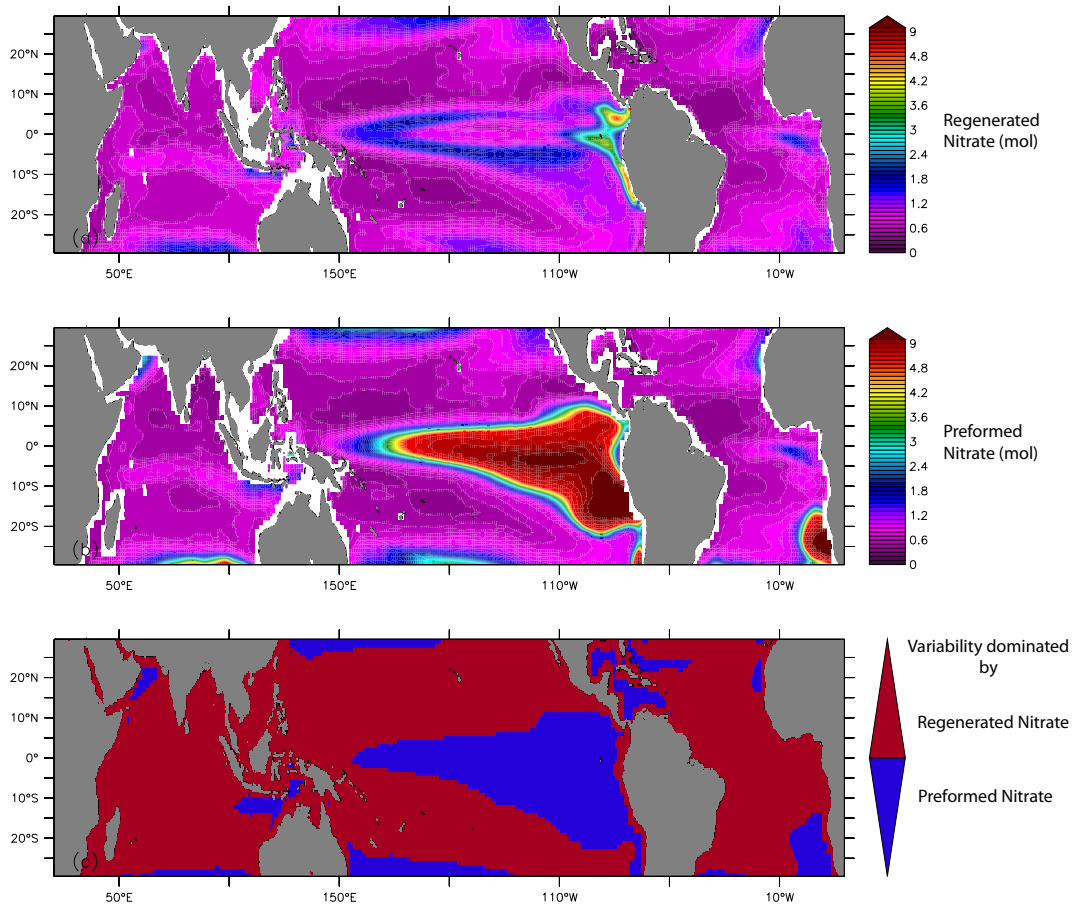

FIGURE 8 – Interannual variability in terms of standard deviation of regenerated nitrate (a, in mol) and preformed nitrate (b, in mol) respectively integrated between the surface and 100 meters. Standard deviation has been computed from the nudged simulation over the 1991-2011 period in the tropical Pacific (30°S-30°N).

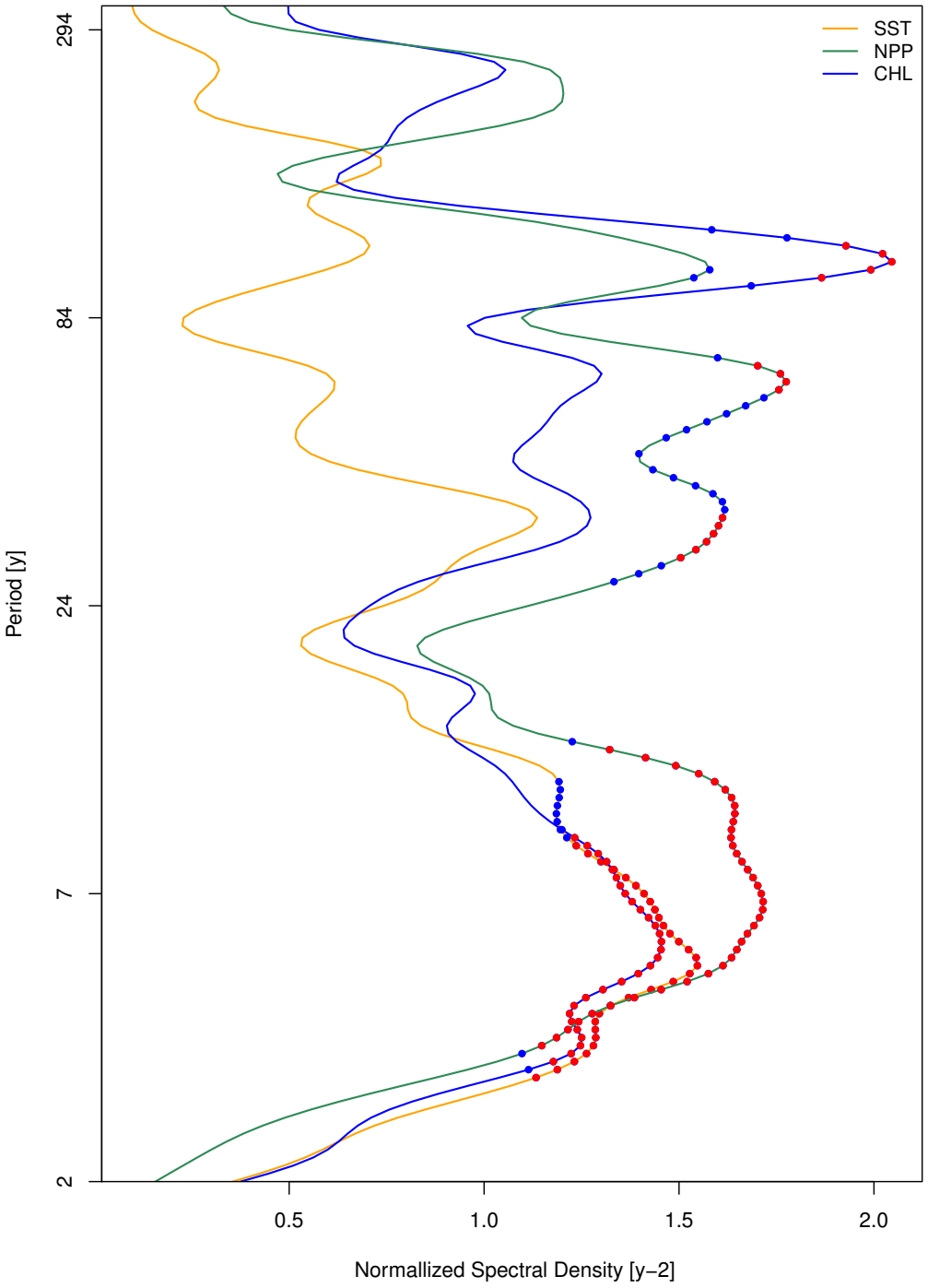

FIGURE 9 – Normalized wavelet Spectrum (in y^{-2}) for sea surface temperature (SST, a), surface chlorophyll (CHL, b) and net primary productivity (NPP, c) in the Tropical Pacific (30°S–30°N) for the 1000-year-long preindustrial simulation performed with IPSL-CM5A-LR. Red and blue dots indicate respectively the significance at 90% and 95% tested against a red noise spectrum.

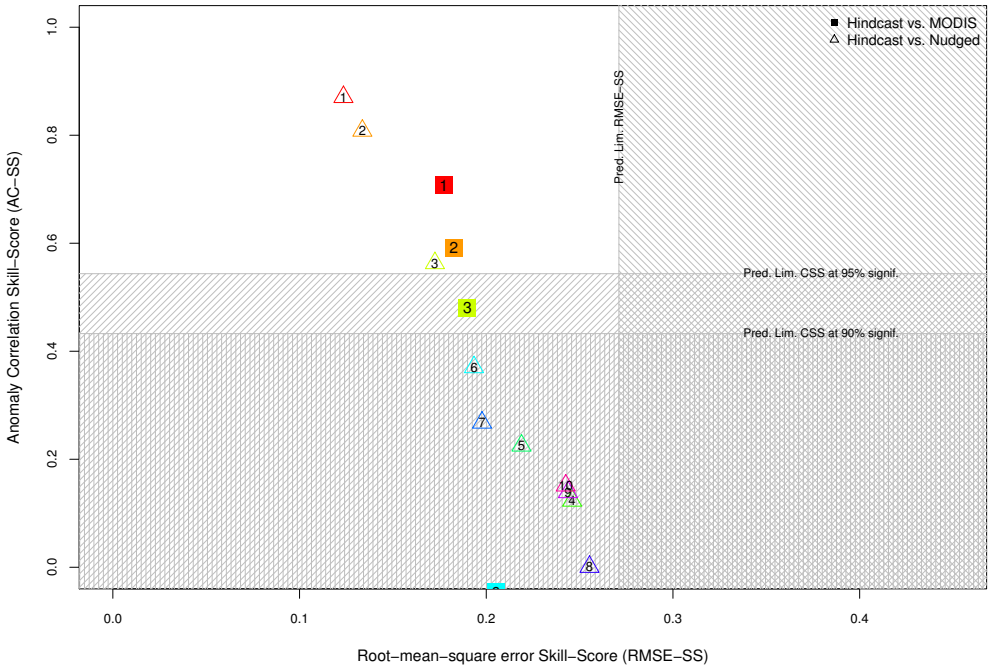

FIGURE 10 – As Figure 2c, but for MODIS measurement of NPP over the whole 2003-2011 period.

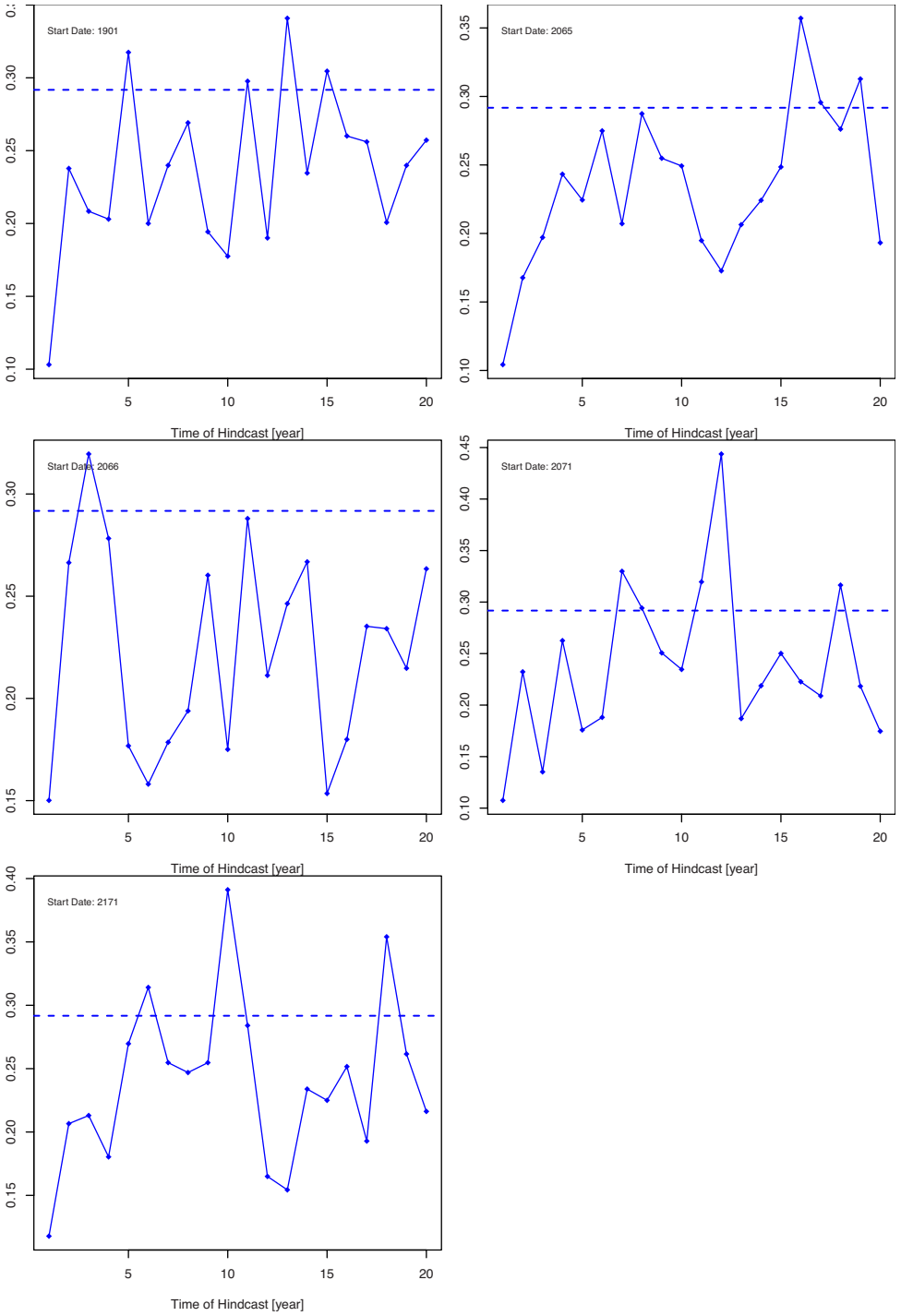

FIGURE 11 – Evolution of the root-mean-squared error (RMSE), for NPP at the five starting dates. The corresponding baseline (see Equations 1) is indicated with blue dashed lines.